© ESO 2018

Multiwavelength campaign on Mrk 509:
XI. Reverberation of the Fe Kα line

G. Ponti[1], M. Cappi[2], E. Costantini[3], S. Bianchi[4], J.S. Kaastra[3,5], B. De Marco[2,6], R. P. Fender[1], P.-O. Petrucci[7], G.A. Kriss[8,9], K.C. Steenbrugge[10,11], N. Arav[12], E. Behar[13], G. Branduardi-Raymont[14], M. Dadina[2], J. Ebrero[3], P. Lubiński[15], M. Mehdipour[14], S. Paltani[16], C. Pinto[3], and F. Tombesi[17,18]

[1] School of Physics and Astronomy, University of Southampton, Highfield, Southampton SO17 1BJ
[2] INAF-IASF Bologna, Via Gobetti 101, 40129 Bologna, Italy
[3] SRON Netherlands Institute for Space Research, Sorbonnelaan 2, 3584 CA Utrecht, the Netherlands
[4] Dipartimento di Fisica, Università degli Studi Roma Tre, via della Vasca Navale 84, 00146 Roma, Italy
[5] Sterrenkundig Instituut, Universiteit Utrecht, P.O. Box 80000, 3508 TA Utrecht, the Netherlands
[6] Centro de Astrobiología (CSIC-INTA), Dep. de Astrofísica; LAEFF, PO Box 78, E-28691, Villanueva de la Cañada, Madrid, Spain
[7] UJF-Grenoble 1 / CNRS-INSU, Institut de Planétologie et d'Astrophysique de Grenoble (IPAG) UMR 5274, Grenoble, F-38041, France
[8] Space Telescope Science Institute, 3700 San Martin Drive, Baltimore, MD 21218, USA
[9] Department of Physics and Astronomy, The Johns Hopkins University, Baltimore, MD 21218, USA
[10] Instituto de Astronomía, Universidad Católica del Norte, Avenida Angamos 0610, Casilla 1280, Antofagasta, Chile
[11] Department of Physics, University of Oxford, Keble Road, Oxford OX1 3RH, UK
[12] Department of Physics, Virginia Tech, Blacksburg, VA 24061, USA
[13] Department of Physics, Technion-Israel Institute of Technology, Haifa 32000, Israel
[14] Mullard Space Science Laboratory, University College London, Holmbury St. Mary, Dorking, Surrey, RH5 6NT, UK
[15] Centrum Astronomiczne im. M. Kopernika, Rabiańska 8, PL-87-100 Toruń, Poland
[16] ISDC Data Centre for Astrophysics, Astronomical Observatory of the University of Geneva, 16, ch. d'Ecogia, 1290 Versoix, Switzerland
[17] Department of Astronomy and CRESST, University of Maryland, College Park, MD 20742, USA
[18] X-ray Astrophysics Laboratory, NASA/Goddard Space Flight Center, Greenbelt, MD, 20771, USA

Preprint online version: November 14, 2018

ABSTRACT

Context. We report on a detailed study of the Fe K emission/absorption complex in the nearby, bright Seyfert 1 galaxy Mrk 509. The study is part of an extensive *XMM-Newton* monitoring consisting of 10 pointings ($\sim$ 60 ks each) about once every four days, and includes also a reanalysis of previous *XMM-Newton* and *Chandra* observations.
Aims. We aim at understanding the origin and location of the Fe K emission and absorption regions.
Methods. We combine the results of time-resolved spectral analysis on both short and long time-scales including model independent rms spectra.
Results. Mrk 509 shows a clear (EW= 58 ± 4 eV) neutral Fe Kα emission line that can be decomposed into a narrow (σ = 0.027 keV) component (found in the *Chandra* HETG data) plus a resolved (σ = 0.22 keV) component. We find the first successful measurement of a linear correlation between the intensity of the resolved line component and the 3-10 keV flux variations on time-scales of years down to a few days. The Fe Kα reverberates the hard X-ray continuum without any measurable lag, suggesting that the region producing the resolved Fe Kα component is located within a few light days-week ($r \lesssim 10^3$ r_g) from the Black Hole (BH). The lack of a redshifted wing in the line poses a lower limit of $\geq$40 r_g for its distance from the BH. The Fe Kα could thus be emitted from the inner regions of the BLR, i.e. within the ~80 light days indicated by the Hβ line measurements. In addition to these two neutral Fe Kα components, we confirm the detection of weak (EW~ $8 - 20$ eV) ionised Fe K emission. This ionised line can be modeled with either a blend of two narrow Fe XXV and Fe XXVI emission lines (possibly produced by scattering from distant material) or with a single relativistic line produced, in an ionised disc, down to a few r_g from the BH. In the latter interpretation, the presence of an ionised standard α-disc, down to a few r_g, is consistent with the source high Eddington ratio. Finally, we observe a weakening/disappearing of the medium and high velocity high ionisation Fe K wind features found in previous *XMM-Newton* observations.
Conclusions. This campaign has made possible the first reverberation measurement of the resolved component of the Fe Kα line, from which we can infer a location for the bulk of its emission at a distance of r~ $40 - 1000$ r_g from the BH.

Key words. galaxies: individual: Mrk 509 – galaxies: active – galaxies: Seyfert – X-rays: galaxies

1. Introduction

X-ray observations of AGN have shown the almost ubiquitous presence of the Fe Kα line at 6.4 keV (Yaqoob et al. 2004; Nandra et al. 1997; 2007; Bianchi et al. 2007; de la Calle et al. 2010). Unlike the optical-UV lines that are emitted by distant

material only, the Fe Kα line traces reflection not only from distant material (such as the inner wall of the molecular torus, the broad line region and/or the outer disc) but also from regions as close as a few r_g (where $r_g = GM/c^2$) from the BH (Fabian et al. 2000).

The powerful reverberation mapping technique, routinely exploited on optical-UV lines (Clavel et al. 1991; Peterson 1993; Kaspi et al. 2000; Peterson et al. 2004), can also be applied to X-ray lines such as the Fe Kα line. This kind of analysis has a tremendous potential, allowing us to map the geometry of matter surrounding the BH, starting from distances of a few gravitational radii up to light years. However, each Fe Kα component is expected to respond on a different characteristic time (years-decades for the torus, several days-months for the BLR-outer disc, and tens of seconds to a few hours for the inner accretion disc) and current X-ray instruments cannot easily disentangle the different components. Indeed, reverberation mapping of all Fe Kα emission components represents an enormous observational challenge, and specially tailored monitoring campaigns (to sample the proper time scales) have to be designed.

Since the detection of the first clear example of a broad and skewed Fe line profile in the spectrum of an AGN (indicating that most of the line emission is produced within few tens of r_g; e.g. MCG-6-30-15, Tanaka et al. 1995) the quest to understand how the broad Fe Kα line varies with the continuum is ongoing. Indeed, close to the BH the simple one-to-one correlation between continuum and reflection line is distorted by General and Special relativistic effects. Several papers present extensive theoretical computations to describe the inner disc reverberation to the continuum taking into account all relativistic effects (Reynolds et al. 1999; Fabian et al. 2000; Reynolds & Nowak 2003).

Several techniques have been employed to measure the variability-reverberation of the relativistic Fe Kα line. However, for the best cases such as MCG-6-30-15, the relativistic Fe line showed a complex behaviour, having a variable intensity at low fluxes (Ponti et al. 2004; Reynolds et al. 2004) while showing a constant intensity at higher fluxes (Vaughan et al. 2003; 2004; see also the case of NG4051: Ponti et al. 2006). This puzzling and unexpected behaviour has been interpreted as due to strong light bending effects by some authors (Miniutti et al. 2003; 2004) or, alternatively, as the evidence that the broad wing of the Fe Kα line is produced by strong and complex absorption effects (Miller et al. 2008).

Thanks to the application of Fe Kα excess emission maps (Iwasawa et al. 2005; Dovciak et al. 2004; De Marco et al. 2009), it has been possible to track weaker coherent patterns of Fe Kα variations. In a few sources Fe Kα variations are consistent with being produced by orbiting spots at a few r_g from the BH (Iwasawa et al. 2004; Turner et al. 2006; Petrucci et al. 2007; Tombesi et al. 2007). Future larger area telescopes are needed to finally assess if these features are present only sporadically during peculiar periods or if, instead, although weak, are always present and can be used to map the inner disc (see e.g. Vaughan et al. 2008; De Marco et al. 2009).

A leap forward in X-ray reverberation studies occurred thanks to the application of pure timing techniques to the long *XMM-Newton* observation of 1H0707-495 that allowed the discovery of a "reverberation lag" between the direct X-ray continuum and the soft excess, probably dominated by FeL line emission (Fabian et al. 2009; Zoghbi et al. 2010). Soon after similar delays were seen in a few other objects (Ponti et al. 2010; De Marco 2011; Emmanouloulos et al. 2011; Zoghbi & Fabian 2011; Turner et al. 2011). Recently, De Marco et al. (2012)

showed that these lags are ubiquitous in AGN, that they scale with M_{BH} and have amplitudes of the order of the light crossing time of a few r_g, thus suggesting a reverberation origin of the delay (but see also Miller et al. 2010). Another fundamental step forward will be to combine these timing techniques to detect reverberation lags in the Fe K band (see Zoghbi et al. 2012).

Reverberation from distant material has the advantage that the intensity of the Fe Kα line and the continuum are expected to follow a simple one-to-one correlation, however, the expected delays between the reflection component and the direct emission are usually too large for a typical X-ray exposure. In fact, reflection from the inner walls of a molecular torus is expected to be delayed by a few years up to several decades and thus requires a very long monitoring campaign. Reflection from the BLR and/or outer disc is more accessible, the delay between continuum and reflection is expected to be between a few days up to few months. Thus a properly tailored monitoring campaign on a bright AGN with *XMM-Newton*, *Chandra* or *Suzaku* could achieve this goal. Several attempts have been made (Markowitz et al. 2003; Yaqoob et al. 2005; Liu et al. 2010). However, the 15-20 % or larger error on the flux of the Fe Kα line and the low-sampling frequency of the X-ray observations have made the application of reverberation of the Fe Kα line on weeks-months timescales basically impossible, until now.

Mrk 509 (z=0.034397) is one of the brightest Seyfert 1 galaxies of the (2–100 keV) X-ray sky (Malizia et al. 1999; Revnivtsev et al. 2004; Sazonov et al. 2007), thus it has been observed by all major X-ray/Gamma-ray satellites. The *Chandra* HETG spectrum shows a narrow component of the Fe K line with an Equivalent Width (EW) of 50 eV (Yaqoob et al. 2004). *XMM-Newton* and *Suzaku* data provide evidence for a second broader ($\sigma = 0.12$ keV) neutral Fe K line (Ponti et al. 2009) as well as a weak ionized emission feature between 6.7–6.9 keV (Pounds et al. 2001; Page et al. 2003; Ponti et al. 2009). The ionised emission can be fit either using a relativistically broadened ionised line or an outflowing photo-ionised gas component.

Imprinted on the Fe K band emission of Mrk 509 are the fingerprints of two kinds of ionised absorption components, one marginally consistent with a medium velocity outflow (v∼ 14000 km s^{-1}; Ponti et al. 2009) and the others out(in)flowing with relativistic velocities (Cappi et al. 2009; Dadina et al. 2005; Tombesi et al. 2010).

Here, we present the spectral and variability analysis of the Fe K complex energy band of Mrk 509 using the set of 10 *XMM-Newton* observations (60 ks each), about one every fours days and spanning more than 1 month, which we obtained in 2009 (see the 3-10 keV light curve in Fig. 1). We also re-analyse the previous 5 *XMM-Newton* observations. Thanks to this extensive monitoring campaign we can measure correlated variations between the Fe K line intensity and X-ray continuum flux, allowing us, for the first time, to perform a reverberation mapping study on this X-ray emission line. In addition we can study the presence of highly ionised matter from the innermost regions around the BH.

The paper is organised as follows. §2 is devoted to the description of the observations and data reduction. In §3 a first parametrisation (with a single Gaussian profile for the Fe Kα line) of the total summed spectrum of the 2009 campaign is presented. Section 4 is dedicated to the detailed study of the Fe Kα emission. We first present the study of the Fe Kα line variability, assuming a single Gaussian profile (§4.1) we then use the *Chandra* HETG data (§4.2) to decompose the Fe Kα line in two Gaussian (narrow and resolved) components. §4.3 presents the correlation between Fe Kα intensity and the 3-10 keV contin-
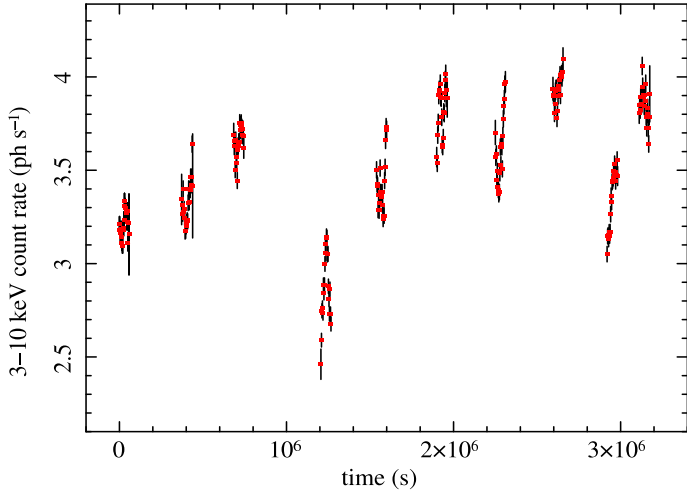
Fig. 1. 3-10 keV EPIC-pn light curve (3 ks time bins) of the 10 *XMM-Newton* observations of the 2009 monitoring campaign.

uum (once the Fe Kα line is fitted with 2 Gaussian lines) which is confirmed, in a model independent way, by the rms spectrum (§4.4). In §4.5 we discuss the possible origin of the Fe Kα line. §5 presents the study and the discussion of the origin of the ionised Fe K emission/absorption. Conclusions are in §6.

2. Observations and data reduction

Mrk 509 was observed for a total of 15 times by *XMM-Newton*: on 2000–10–25, 2001–04–20, 2005–10–16, 2005–10–20, 2006–04–25, and 10 times in 2009 (see Fig. 1 starting from 2009-10-15 and ending on 2009-11-20). Ponti et al. (2009) and Kaastra et al. (2011) provide a full description of the first 5 and the last 10 *XMM-Newton* observations, respectively.

We initially reduced the EPIC data (as in Mehdipour et al. 2011), starting from the ODF files, using the standard SAS v9.0 software. However, we noted that the rest-frame best fit energy of the Fe Kα line in the EPIC-pn spectrum ($E_{FeK\alpha} = 6.35 \pm 0.01$ keV) was not consistent with the best fit energy in the summed spectrum of the EPIC-MOS data ($E_{FeK\alpha} = 6.41 \pm 0.01$ keV). This discrepancy (~ 50 eV) was found to be systematic, and was present in all 10 observations. Being significantly larger than the reported systematic uncertainty on the calibration of the absolute energy scale of 10 eV (CAL-TN-0018), this result triggered an in-depth study of the pn and MOS energy scales by the *XMM-Newton* EPIC calibration team. After excluding that this effect is related to X-ray loading, a stronger than expected long-term degradation/evolution of the Charge Transfer Inefficiency (CTI) was found. The pn long-term CTI was thus re-calibrated, and its corrected value implemented in the SAS version 10.0.0 (see CCF release note XMM-CCF-REL-271 [1]).

The EPIC data were thus reduced again using the SAS version 10.0.0. During the XMM-Newton monitoring, both the EPIC-pn and the EPIC-MOS cameras were operating in the Small Window mode with the Thin filter applied. The #XMMEA_EP and #XMMEA_EM, for the pn and MOS cameras, respectively, are used to filter the events lists and to create Good Time Intervals (GTI). The FLAG==0 is then used for selection of events for making the spectra. The data were screened for increased flux of background particles. The contribution due

---

[1] See http://xmm2.esac.esa.int/external/xmm_sw_cal/calib/rel_notes/index.shtml

to soft protons flares was negligible during the whole 2009 monitoring. The final cleaned EPIC-pn exposures for each XMM-Newton observation were about 60 ks, i.e. roughly 40 ks, after accounting for the proper dead-time of the pn when operating in small window mode (see Table 1 of Mehdipour et al. 2011, for a list of the exposure times).

The pn and MOS spectra were extracted from a circular region of 45″ and 20″ radius centred on the source, respectively. The background was taken locally from identical circular regions located on the same CCD of the source for the EPIC-pn but on another CCD for the EPIC-MOS. The EPIC data showed no evidence of significant pile-up, thus single and double events were selected for both the pn (PATTERN<=4) and the MOS (PATTERN<=12) camera. Response matrices were generated for each source spectrum using the SAS tasks *arfgen* and *rmfgen*. The sum of the spectra has been performed with the MATHPHA, ADDRMF and ADDARF tools within the HEASOFT package (version 6.10).

Mrk509 was observed by the Chandra Advanced CCD Imaging Spectrometer (ACIS: Garmire et al. 2003) with the High-Energy Transmission Grating Spectrometer (HETGS: Canizares et al. 2005) in the focal plane, on 2001, April 13th (obsid 2087). Data were reduced with the Chandra Interactive Analysis of Observations (CIAO: Fruscione et al. 2006) 4.2 and the Chandra Calibration DataBase (CALDB) 4.3.1 software, adopting standard procedures.

All spectral fits were performed using the Xspec software (version 12.3.0) and include the neutral Galactic absorption (4.44×10^{20} cm^{-2}; Murphy et al. 1996), the energies are in the rest frame if not specified otherwise, however the energies in the plots are in the observed frame and the errors are reported at the 90 per cent confidence level for one interesting parameter (Avni 1976) in all the tables, while they are 1 σ errors in the Figures. Mrk 509 has a cosmological redshift of 0.034397 (Huchra et al. 1993) corresponding to a luminosity distance of 145 Mpc (taking $< H_0 >= 73$ km s^{-1} Mpc^{-1}, $\Omega_\Lambda = 0.73$ and $\Omega_m = 0.27$).

3. The mean spectrum

The upper panel of Figure 2 shows the data to best fit model ratio plot of the summed spectra of the 10 EPIC-pn observations performed during the 2009 *XMM-Newton* monitoring campaign, fitted in the 3.5-5 and 7.5-10 keV band with a simple power law, absorbed by Galactic material (interstellar neutral gas; PHABS model in XSPEC). For comparison, the black data points in the lower panel of Fig. 2 show the same plot for the summed EPIC-pn spectrum of the previous 5 *XMM-Newton* observations taken between 2000 and 2006, while the red data show the summed XIS0+XIS3 spectra of the 4 *Suzaku* observations performed between April and November 2006 (see Ponti et al. 2009 for more details).

Thanks to a longer integrated exposure and a slightly higher flux, the source spectrum in the FeK band has significantly better statistics during the 2009 campaign than the sum of all the previous observations (see Fig. 2). Hence we can better constrain the FeK complex and study its variability not only on the timescales of days and weeks over which the monitoring has been performed, but also on time-scales of years, using previous observations.

The upper panel of Fig. 2 shows, as observed during previous observations, an evident emission line at 6.4 keV as well as an emission tail at higher energies. A simple power law fit to the 4-10 keV total pn spectrum gives an un-acceptable fit ($\chi^2 = 2445.7$ for 1197 dof). Adding a Gaussian line to fit the Fe Kα line at 6.4
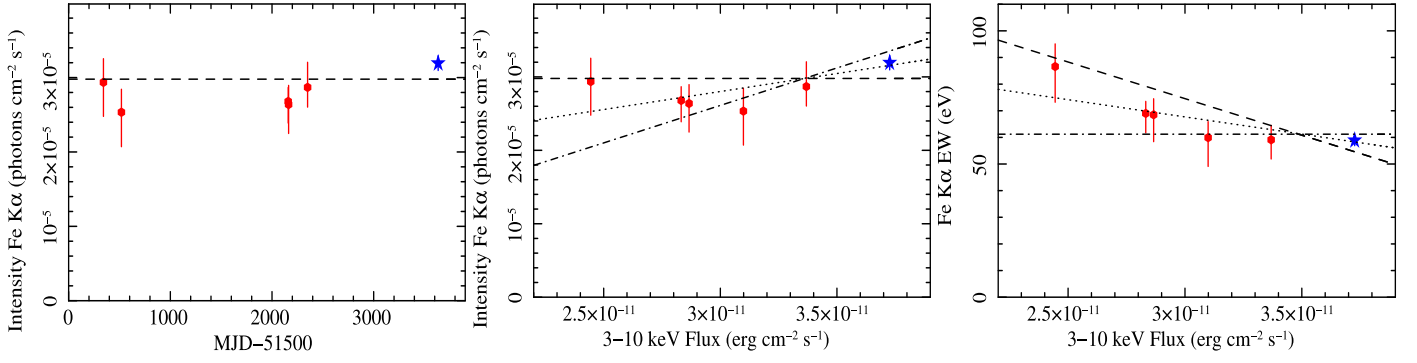
Fig. 3. *(Left, middle and right panels)* Intensity vs. time in MJD, intensity vs. 3-10 keV flux and EW vs. 3-10 keV flux of the Fe Kα line fitted with a single Gaussian profile with σ = 0.092 keV (model 1), respectively. Each data point represents the best fit result obtained from the fit of the spectrum of each *XMM-Newton* observation (red hexagonals) and the total spectrum of the 2009 data (blue stars). The dashed lines represent the expected relations if the Fe Kα line has constant intensity, while the dash-dotted lines represent a constant EW, and the dotted line shows the best fit trend. The left panel show the observation date in Modified Julian Date, MJD minus 51500 which corresponds to 1999 November 18th. Two *XMM-Newton* observations occur at day 2159 and 2163 and appear overlapping in the left panel.

keV improves the fit by $\Delta\chi^2$ = 1134 for 3 extra parameters (see model 1 in Tab. 1). This line reproduces the bulk of the neutral FeK emission (E = 6.43 ± 0.01 keV), but leaves strong residuals at higher energies which might be, at least in part, associated with an Fe Kβ emission line. We thus add a second line with the same line width as the Fe Kα line and an energy of 7.06 keV (Kaastra & Mewe 1993). The best fit parameters are given as model 2 in Tab. 1, and the fit improves by $\Delta\chi^2$ = 66.9 for the addition of 1 new parameter. The best fit intensity is $N_{Fe\,K\beta}$ = 0.75×10^{-5} ph cm^{-2} s^{-1}, and the observed Kβ/Kα ratio is = 0.19 ± 0.02. This is slightly, but significantly, higher than 0.155-0.16, the value estimated by Molendi et al. (2003; who assume the Basko 1978 formulae; but see also Palmeri et al. 2003a,b). The excess of Fe Kβ emission might be due to the contamination by the Fe XXVI emission line at 6.966 keV. This idea is further supported by the observation of clear residuals, in the best fit, around 6.7 keV; and by the best fit FeK energy (E = 6.43 ± 0.01 keV) which is inconsistent with the line arising from neutral iron. This thus suggests that the Gaussian line is trying to fit both the neutral and ionised Fe K components.

To model ionised FeK emission, we add two narrow (σ = 0) emission lines, one (Fe XXV) emitting between 6.637 and 6.7 keV (to take into account emission for each component of the triplet) and the other (Fe XXVI) emitting at 6.966 keV (model 3 in Tab. 1). Moreover we impose that the intensity of the Kβ has to be 0.155-0.16 times the intensity of Fe Kα one (and $\sigma_{Fe\,K\beta} = \sigma_{Fe\,K\alpha}$). The fit significantly improves ($\Delta\chi^2$ = 25 for the addition of one more parameter). Both Fe XXV (the best fit line energy is consistent with each one of the triplet) and Fe XXVI are statistically required (although the Fe XXVI line is not resolved from the Fe Kβ emission, thus its intensity depends on the assumed Kα/Kβ ratio). In this model the Fe Kα line is roughly consistent with being produced by neutral or lowly ionised material ($E_{FeK\alpha}$ = 6.415 ± 0.012 keV).

Pounds et al. (2001), Ponti et al. (2009), de la Calle et al. (2010), Cerruti et al. (2011) and Noda et al. (2011) suggest that the inner accretion disc in Mrk509 might be highly ionised and thus the ionised emission of the Fe K complex might be associated to a relativistic ionised reflection component produced in the inner disc. To test this hypothesis, we substitute the two narrow lines (Fe XXV and Fe XXVI) with one broad ionised line (model 4 in Tab. 1) with a relativistic profile (disc line profile

for a Schwarzschild black hole; *diskline* model in *Xspec*). We fixed the line energy either to 6.7 or 6.96 keV (for the Fe XXV or Fe XXVI line, respectively) and the inner and outer disc radius to 6 and 1000 gravitational radii. In both cases the best fit with this model suggests the inner accretion disc to be moderately inclined $\sim$ 33 − 18°, to have a fairly standard disc emissivity index −2.2 − 2.8 and an equivalent width of the line to be EW$\sim$ 36 − 40 eV. The data are described reasonably well by this model resulting in a χ^2 = 1216.0 and χ^2 = 1219.4 for 1191 dof, for the case of a broad Fe XXV and Fe XXVI line, respectively. Thus, the single broad ionised disc-line model is statistically indistinguishable from the multiple narrow lines one (χ^2 = 1219.8 for 1192 dof).

3.1. Medium velocity-high ionisation winds

The summed spectrum of the previous *XMM-Newton* observations showed a medium velocity ($v_{out} \sim$ 0.048 ± 0.013 c) highly ionised (Log(ξ)$\sim$ 5) outflow in Mrk 509 (Ponti et al. 2009). The associated Fe XXVI absorption line was detected both in the EPIC-pn and MOS camera, with an equivalent width EW= $-13.1^{+5.9}_{-2.9}$ eV and with a total significance between 3 − 4σ ($\sim$ 99.9 % probability).

During the 2009 *XMM-Newton* campaign this highly ionised absorption component is not significantly detected. If we add a narrow Gaussian absorption line at 7.3 keV, the energy of the absorption feature in the previous *XMM-Newton* observations, we observe the line to be much weaker with the best fit line EW being $-3.2^{+2.6}_{-2.8}$ eV, significantly smaller than observed in previous *XMM-Newton* observations.

4. The neutral Fe Kα component

In this section we further investigate the nature of the Fe Kα line, looking at the individual spectra obtained over the years. Our analysis of the long 2009 monitoring campaign, which triples the total exposure on Mrk509, confirms the presence of a resolved component (σ = 0.092 ± 0.012 keV) of the neutral Fe Kα line (see model 3, but also 4 and 5 of Tab. 1).
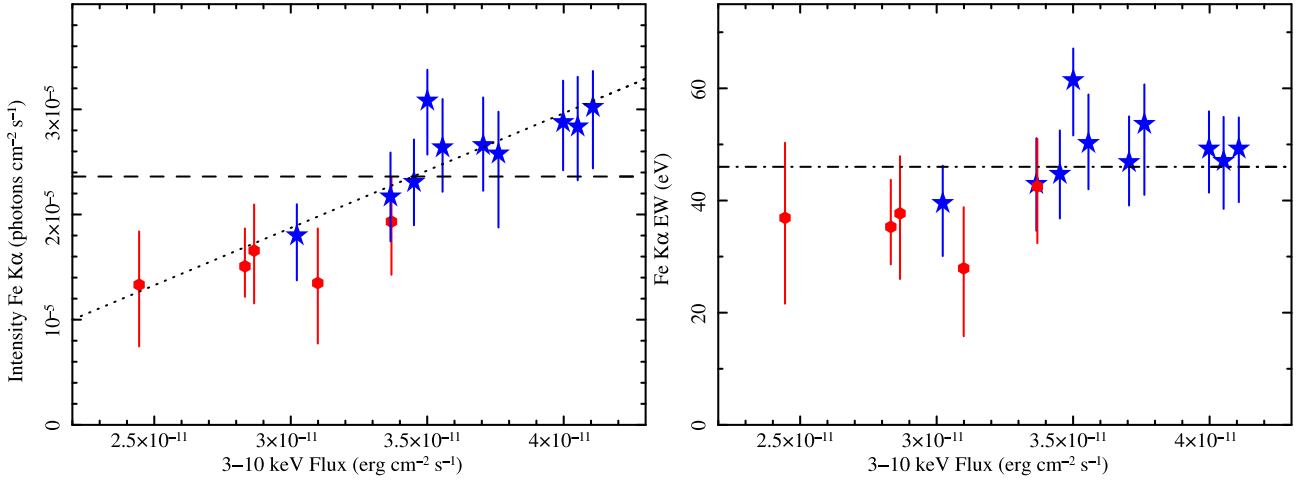
Fig. 4. *(Left and right panel)* The intensity and EW of the resolved ($\sigma = 0.22$ keV) Fe Kα component (the narrow Fe Kα component is assumed to have $\sigma = 0.027$ keV and be constant) as a function of the 3-10 keV flux. Blue stars and red hexagonals show the best fit results of the 10 observations of the 2009 campaign and of the previous *XMM-Newton* observations, respectively. Dashed and dot dashed lines show the constant intensity and constant EW cases, respectively. The best fit relation (dotted line) is consistent with the resolved component of the Fe Kα line having constant EW. The intensity of the resolved component of the Fe Kα line follows the 3-10 keV continuum variations with a 1-to-1 relation.

4.1. Fe Kα variations on years time-scales

To study the variability of the neutral Fe Kα emission line (on years time-scales), we fit the spectrum of each of the old *XMM-Newton* observations (i.e. between 2000 and 2006) with a single FeKα (plus associated Kβ emission) plus two narrow emission lines (such as in §3 in model 3) to parametrize the ionised FeK emission (see Tab. 1). Leaving the Fe Kα widths free to vary, as in Tab. 1, would result in unconstrained values for the spectra with the shortest exposures (due to the lower statistics). We thus decide to fix the width of the Fe Kα line to $\sigma = 0.092$ keV, its best fit value as observed in the total spectrum of the 2009 campaign (model 3 of Tab. 1).

The left panel of Fig. 3 shows the Fe Kα line intensity for each *XMM-Newton* observation as a function of time, using the summed 2009 data. The line intensity is observed to vary by less than 25 %. The fit with a constant Fe Kα intensity (dashed line), however, is unsatisfactory ($\chi^2 = 10.7$ for 5 dof). The middle panel of Fig. 3 shows the Fe Kα intensity vs. source flux in the 3-10 keV band. The fit slightly improves when a linear relation (see dotted line) is considered ($\Delta\chi^2 = 7.6$ for the addition of one more parameter; 97 % F-test probability). The increase in Fe Kα intensity with flux might suggest that the line is responding quickly to the illuminating continuum, keeping a constant EW with flux. The dash-dotted line shows the expected Fe Kα intensity variation for a line with constant EW. The observed line intensity variations are intermediate between the constant intensity and constant EW cases. The right panel of Fig. 3 confirms that the line has neither a constant intensity nor constant EW, instead it sits somewhere in the middle between these two cases.

The Fe Kα variations on years time-scales suggest that at least part of the line is varying following the 3-10 keV continuum. We want to point out that the width of the Fe Kα line is comparable to the EPIC-pn energy resolution. This means that the observed Fe Kα variability may be the product of a constant narrow component, coming from distant material, plus a broader, resolved and variable Fe Kα line produced closer to the BH. Unfortunately, due to the limited energy resolution of the EPIC cameras aboard *XMM-Newton*, we cannot resolve the Fe K emission, coming from regions located at light weeks from those

at light years from the BH, based on the Fe Kα line widths. Only with the *Chandra* high energy transmission grating (HETG) we can confidently pose some constraints on the distance of the different Fe K emission components.

4.2. Chandra HETG

Chandra observed Mrk 509 with the HETG instrument only once for 50 ks (Yaqoob et al. 2003). During the HETG observation the 3-10 keV flux was 4.36×10^{-11} erg cm^{-2} s^{-1} with a power law spectrum of index $\Gamma = 1.76^{+0.03}_{-0.02}$. An excess was present at 6.4 keV, thus we added a Gaussian line[2]. In agreement with the results obtained by Shu, Yaqoob & Wang (2010) and Yaqoob & Padmanabhan (2004) we detect a line at 6.42 ± 0.02 keV with an intensity of $3 \pm 2 \times 10^{-5}$ photons cm^{-2} s^{-1}. The line is resolved and has a width significantly smaller than the one measured by *XMM-Newton*, $\sigma = 0.027^{+0.018}_{-0.010}$ keV. This suggests that, at least part of, the neutral Fe Kα emission is produced in regions more distant than a few thousands gravitational radii. In fact, if the material is in Keplerian motion and assuming a BH mass of Mrk 509 of $M_{BH} = 1.4 - 3 \times 10^8$ M$_\odot$ (Peterson et al. 2004; Mehdipour et al. 2011), then the narrow core of the line is produced at a distance of r=0.2-0.5 pc (~ 30000 r$_g$). We note that this value is of the same order of magnitude as the molecular sublimation radius for Mrk 509. Landt et al. (2011) using quasi-simultaneous near-infrared and optical spectroscopy estimate a radius of the hot dust of ~ 0.27 pc (0.84 ly), which is also consistent with the one estimated following eq. 5 of Barvainis (1987) assuming a bolometric luminosity L$_{Bol} = 1.07 \times 10^{45}$ erg s^{-1} (Woo & Urry 2002). This suggests that this narrow component of the Fe K line might be associated to the inner wall of the molecular torus.

---

[2] In order not to lose the excellent energy resolution, we decided not to rebin the spectrum and to fit the data using the C-statistics (Cash 1979). The best fit has C-stat value of 370.5 for 284 dof.
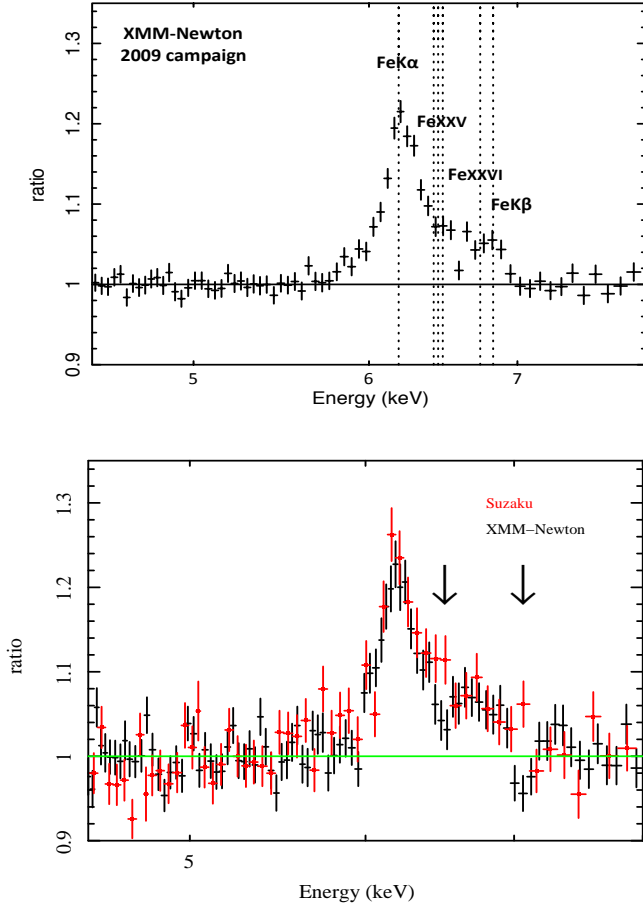
Fig. 2. *(Upper panel)* Summed EPIC-pn spectra of the 10 observations performed during the 2009 *XMM-Newton* monitoring campaign. The data are fit, in the 4-5 and 7.5-10 keV bands, with a simple power law, absorbed by Galactic material, and the ratio of the data to the best-fit model is shown. The dotted lines indicate the rest frame positions of the Fe Kα, Fe Kβ, Fe XXV (resonance, intercombination and forbidden) and Fe XXVI lines. The x-axis reports the observed-frame energy. *(Lower panel)* In red the 2006 XIS0+XIS3 *Suzaku* summed mean spectra are shown. In black the summed spectra of the 5 *XMM-Newton* observations performed between 2000 and 2006 are shown. This Figure is taken from Ponti et al. (2009). The arrows mark possible absorption features in the spectrum.

4.3. Two components of the Fe Kα line

Thus, as suggested by the analysis of the *Chandra* HETG data and in agreement with the observed variability on years time-scales, we interpret the Fe Kα line as being composed by two components which are indistinguishable at the EPIC resolution. We first re-fit the mean spectrum of the 2009 campaign with two components for the Fe Kα line. One "narrow" component with the line width fixed at the best fit value derived from *Chandra* analysis ($\sigma = 0.027$ keV) plus a "resolved" component with its width free to vary. Model 6 in Tab. 2 shows the best fit results assuming the energy of both components is the same. The narrow component has a best fit EW= 27 ± 4 eV, while the resolved neutral line has an EW= 42^{+9}_{-4} eV and a best fit line width

$\sigma = 0.22 \pm 0.05$ keV which is larger than the single Gaussian Fe Kα fit ($\sigma = 0.092$ keV).

Reflection is the most probable origin of the Fe Kα line. Associated to reflection lines an underlying reflection continuum is expected and generally observed. In particular the ratio between the intensity of the line over the reflection continuum strongly depends on the reflector column density reaching a value of $EW_{FeK\alpha} \sim 1$ keV for Compton thick materials. To check the impact of the reflection continuum on the best fit model we add a standard neutral reflection continuum (PEXRAV in XSPEC) with intensity such that the $EW_{FeK\alpha} = 1$ keV over their reflection continua. The new best fit line EW do not vary significantly (EW= 26 ± 3 eV and EW= 33^{+8}_{-5} eV, for the narrow and resolved Fe Kα lines, respectively). Thus, and considering also the limited energy band used here we decide to disregard the continuum reflection component (the impact of the reflection component on the broad band source emission will be studied by Petrucci et al. 2012 taking into account the UV to soft Gamma ray emission with physical models). The narrow component, as observed during the 2009 campaign, has an intensity of $1.5 \pm 0.2 \times 10^{-5}$ ph cm^{-2} s^{-1}, which is about half the total Fe Kα intensity (see Tab. 1 and Fig. 3). This value is consistent with the intensity of the narrow Fe Kα line observed by *Chandra*. The width of the narrow component suggests a distance of 0.2-0.5 pc from the BH, thus we expect that all the variability on time-scales shorter than a few years would be smeared out because of light travelling effects. For this reason and because the lower signal to noise in the individual 2009 and earlier *XMM-Newton* spectra does not allow us to disentangle both components, in all the following fits we assume a constant intensity of 1.5×10^{-5} cm^{-2} s^{-1} for this narrow Fe Kα component.

Next, we fit the spectrum of each of the 15 *XMM-Newton* observations with model 6 shown in Tab. 2, assuming a constant intensity for the narrow Fe Kα component and constant width for the resolved component, plus the associated Fe Kβ and narrow Fe XXV and Fe XXVI lines. The left panel of Fig. 4 shows the intensity of the resolved component ($\sigma = 0.22$ keV) vs. the 3-10 keV flux for the 10 observations of the 2009 monitoring (blue stars) as well as for the previous *XMM-Newton* observations (red hexagonals). The dashed line shows the best fit assuming that the Fe Kα intensity is constant, which results in an unsatisfactory fit with $\chi^2 = 33.2$ for 14 dof. On the other hand, once the data are fitted with a linear relation (dotted line), the fit significantly improves ($\Delta\chi^2 = 23.0$ for the addition of 1 new parameter, which corresponds to F-test probability > 99.98 %). We also compute the Pearson's linear correlation coefficient is equal to 0.87 and has a probability = 2.7×10^{-5}, which corresponds to a significance of the correlation of more than 4σ (similar results are obtained using a Spearman's rho or Kendall's tau correlation coefficients). The slope of the observed best fit relation is consistent with that expected if the resolved line is responding linearly to the continuum variations. This is confirmed in the right panel of Fig. 4 which shows the resolved Fe Kα line EW is consistent with being constant ($\chi^2 = 17.1$ for 14 dof), as expected if the Fe Kα line is responding linearly to the 3-10 keV continuum flux variations.

The line intensity is significantly variable even on time-scales of few days, e.g. between the different pointing of the 2009 monitoring campaign. In fact, fitting the 2009 Fe Kα intensities with a constant gives a $\chi^2 = 13.7$ for 9 dof, which becomes $\chi^2 = 5.3$ when a linear relation is considered (as specified in §2, conservative 90 % errors are used here). The Pearson's linear correlation coefficient results to be 0.8 and has a probability
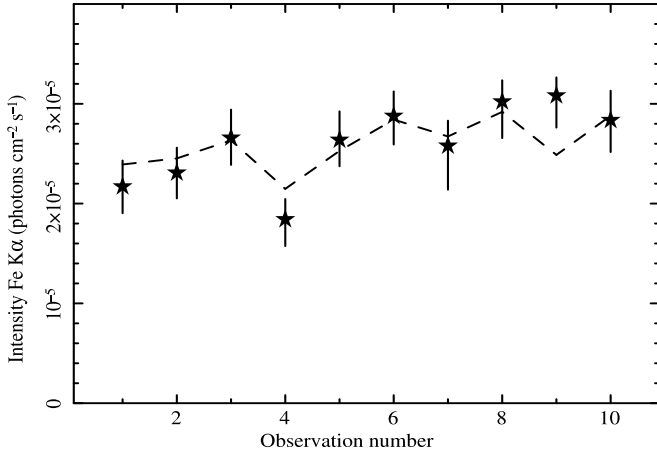
Fig. 5. Intensity vs. observation number of the 10 *XMM-Newton* pointings of the 2009 campaign. The black dashed line shows the re-scaled (with the mean 3-10 keV flux equalling the mean line intensity) 3-10 keV source flux. The intensity of the resolved component of the Fe Kα line follows, with a 1-to-1 relation the 3-10 keV continuum variations without any measurable lag. 1σ errors are shown.
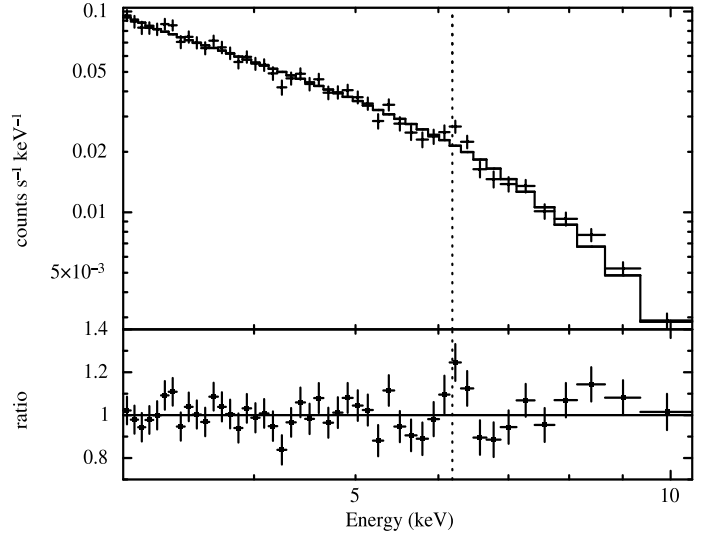

Fig. 6. Long time-scales total rms spectrum between the different observations. The spectrum is calculated with time bins of 60 ks (corresponding to the exposure of each *XMM-Newton* pointing) and the total monitoring time of about 1 month. An excess of variability is clearly evident at 6.4 keV (EW= 71 ± 36 eV). This excess confirms, in a model independent way, the correlated variability of the resolved Fe K line component (see Fig. 5).

= 5×10^{-3}, which corresponds to a significance of the correlation of about 3 σ.

Fig. 5 shows the variations of the intensity of the resolved component of the Fe Kα line as a function of time (1 σ errors are shown here), during the 2009 campaign, overplotted on the 3-10 keV rescaled flux (dashed line). As already suggested above and Fig. 4, the Fe K line variations track that of the continuum very well. We also note that no measurable lag is present, thus this broad component of the Fe Kα line responds to the X-ray continuum within less than four days.

4.4. Total RMS spectra

Figure 6 shows the total Root Mean Square variability (rms) spectrum calculated between the 10 different observations of the 2009 campaign. The rms has been calculated with ten time bins, each one being a 60 ks *XMM-Newton* pointing. Thus this rms is sampling the variability within the observation separation time-scale of about 4 days and the monitoring time-scale of slightly more than one month (see Fig. 1). The total rms shows the spectrum of the variable component, only. Thus, in contrast to the mean spectrum, it has no contribution from the constant emission from distant material (i.e. the narrow core of the Fe K line). The uncertainties on the total rms are derived from the uncertainties on the fractional variability (see formula B.2 of Vaughan et al. 2003; A.1 of Ponti et al. 2004) multiplying for the mean and taking into account its error.

The 3-10 keV total rms spectrum has a power law shape with spectral index Γ = 1.98 ± 0.06 and normalisation of $1.05 \pm 0.05 \times 10^{-3}$ ph. cm^{-2} s^{-1} (see Fig. 6). A clear excess of variability is present at 6.4 keV. The addition of a Gaussian line significantly improves the fit ($\Delta\chi^2$ = 10.6 for the addition of 2 dof, that corresponds to a F-test significance of 99.3 %). The best fit energy of the line is E = 6.45 ± 0.08 keV and intensity $(2 \pm 1) \times 10^{-6}$ ph. cm^{-2} s^{-1}. The width of the line is constrained to be less than $\sim$ 0.2 keV, consistent with the variable resolved neutral Fe K line. The equivalent width in the total rms spectrum is EW = 71 ± 36 eV consistent with the EW of the resolved component observed in the mean spectrum. The detection of this

excess of variability indicates, in a model independent way, that the resolved component of the line is varying linearly with the continuum on these time-scales. This reinforces the robustness of the detection of Fe K reverberation.

4.5. Locating the Fe Kα emitting region

Are the observed variability properties in agreement with the spectral ones? Assuming that the material producing the resolved Fe K line is in Keplerian motion around the BH, the line width (σ = 0.22 keV) implies that it is located at $300 - 1000$ r$_g$ from the BH. Assuming a BH mass of Mrk 509 of M$_{BH}$ = $1.4 - 3 \times 10^8$ M$_\odot$ (Peterson et al. 2004; Mehdipour et al. 2011), then this distance corresponds to about few days - a light week. The typical spacing between the different *XMM-Newton* observations during the 2009 monitoring is about 4 days, thus it is in very good agreement with the observed Fe Kα variations. Moreover, the fast response of the Fe Kα flux to the continuum changes indicates that the bulk of the resolved Fe Kα emission is produced around or within several hundreds up to few thousands gravitational radii from the central BH.

It is more difficult, however, to pose a lower limit to the position of the Fe Kα emitting region. We note that if the Fe Kα line emitting region extends down to few gravitational radii from the BH, then the line shape should present a prominent red wing. Thus, we fit the resolved component of the Fe Kα line with a disc line profile (DISKLINE in *Xspec*). In the fitting process we allow the line energy to vary in the range 6.4-6.42 keV, we fix the disc outer radius to 1000 r$_g$ and the illumination profile to $\alpha = -3$ (the expected value for a standard alpha disc; Laor 1991; Wilkins & Fabian 2011). The lack of relativistic redshifted Fe Kα emission suggests an inner radius larger than $\sim$ 85, 45 and 37 r$_g$ (which corresponds to roughly 8-16 light hours) for a disc inclination of 30, 20 and 10 degrees, respectively. Thus, the resolved component of the Fe Kα line is probably emitted between $40 - 1000$ r$_g$ from the BH.

Can such a "narrow" disc annulus produce an Fe Kα line of $\sim 40 - 50$ eV? Reflection from an accretion disc with Solar iron abundances covering half of the sky is expected to produce a Fe Kα line with EW$\sim 100 - 150$ eV (Matt et al. 1991). The line EW is expected to decrease/increase roughly linearly/logarithmically for iron abundances lower/higher than Solar (Matt et al. 1996; 1997). Steenbrugge et al. (2011) measured in Mrk 509 a relative iron to oxygen abundance of Fe/O= 0.85 ± 0.06. Assuming that this translate into an iron abundance of 0.85 Solar (but see Arav et al. 2007), this would correspond to EW$_{\mathrm{FeK}\alpha} \sim 90 - 130$ eV. If the primary X-ray source in Mrk 509 is compact (as the variability suggests; McHardy et al. 2006; Ponti et al. 2012) and located at a few r_g above the BH and if the disc is flat, we can estimate (neglecting relativistic effects) the geometric solid angle covered by the disc annulus producing the Fe Kα line ($r_{\mathrm{in}} \sim 40$ and $r_{\mathrm{out}} \sim 1000$ r_g). If the primary X-ray source is located between 1 and 4 r_g above the BH (De Marco et al. 2012), the flat disc annulus covering factor would be between 2 and 5 % of the sky. Thus reflection from such a flat annulus would produce (even in the extreme case of a Fe Kα EW= 130 eV for a standard disc) a line with EW$\sim 4 - 13$ eV. The observed EW of the resolved-variable Fe Kα line is several times larger (EW=42 eV) than this estimated value. This indicates a larger covering factor of the reflector, compared to the flat disc, suggesting that the material producing the Fe Kα line is distributed azimuthally above the disc, possibly in the form of clouds, perhaps associated to the inner BLR (see Costantini et al. 2012 for more details).

The observed correlation on days-weeks timescales constraints also in which part of the BLR the Fe Kα line is produced. We can exclude, in fact, that the Fe Kα emission is produced in the optical BLR (producing the bulk of Hβ emission), because the Hβ line is observed to reverberate with a delay of 80 days, being thus significantly more distant than the region producing the Fe Kα line. On the other hand, several studies show that the BLR might be stratified, with the higher ionisation lines located closer to the central BH. The correspondence between Fe Kα and the inner BLR is reinforced by the consistency between the width of the Fe Kα line ($\sigma = 0.21 \pm 0.07$ keV, which corresponds to $FWHM \sim 1.5 - 3 \times 10^4$ km s^{-1}) and the ones of the broadest components of the UV broad emission lines (e.g. Lyα, C IV, C III and O VI) which have components with $FWHM \sim 10^4$ km s^{-1} (Kriss et al. 2011).

The lack of relativistic effects on the shape of the Fe Kα line suggests the absence of a neutral standard thin accretion disc extending down to a few gravitational radii from the BH. However, this appears to be at odds with the high efficiency ($L_{\mathrm{Bol}} \sim 5 - 10$ % L_{Edd}) of the disc emission of Mrk 509 (Mehdipour et al. 2011; Petrucci et al. 2012). This leads to the question of why we do not find traces of the inner accretion disc in the Fe Kα line shape if it is present in this source.

5. The ionised Fe K emission

During both the 2009 campaign and the previous *XMM-Newton* observations, Mrk 509 clearly showed an excess of emission around 6.7-7 keV (see Fig. 2) most probably associated to emission from ionised iron. As shown in §3 this excess can be modelled both by the combination of narrow emission lines from Fe XXV and Fe XXVI, or by a single relativistic emission line (see Tab. 1). The parameters of this weak ionised emission line(s) can be affected by the modelling of the stronger Fe Kα line. For this reason, we now re-fit the mean spectrum including both the narrow and the resolved component of the Fe Kα line.

We first consider that the ionised emission is produced by narrow emission lines (Fe XXV and Fe XXVI). Such emission lines from highly ionised ions are now often observed (Costantini et al. 2010; e.g. for a compilation of sources, Bianchi et al. 2009a,b; Fukazawa et al. 2011) and they can arise from photo-ionised (Bianchi et al. 2005; Bianchi & Matt 2002) or collisionally ionised plasma (Cappi et al. 1999). Thus we fit the spectrum with two components for the Fe Kα line and the associated Kβ lines, plus two narrow ($\sigma = 1$ eV) Gaussian emission lines one (Fe XXV) with energy constrained to be between 6.637 and 6.7 keV and the other (Fe XXVI) with energy fixed at $E = 6.966$ keV (see model 6 in Tab. 2). The model reproduces the data well ($\chi^2 = 1198.5$ for 1190 dof). The weakness of the Fe XXV and Fe XXVI lines prevents us from significantly constraining the line variability between the different *XMM-Newton* observations.

For comparison, we fit with the same model also to the summed spectrum of all *XMM-Newton* observations taken between 2000 and 2006 (see model 7 of Tab. 2). The ionised emission lines are consistent with being constant within the two sets of observations. However, the statistics is not good enough to discriminate if it is the line intensity (which would suggest an origin at large distances) or the EWs remain constant. Clear is, instead, the variation of the medium outflow velocity highly ionised absorption line, which almost disappeared during the 2009 campaign. The addition of this component to the model used to fit the combined spectra of the 2009 campaign, improves the fit by $\Delta\chi^2 = 4.5$ for 2 new parameters which corresponds to a F-test probability of ~ 90 %. Thus we decide to disregard this absorption component in all subsequent fits.

Another clear difference compared to previous observations is related to the disappearance of the highly ionised absorption with mildly relativistic (up to 0.14-0.2c) outflow velocities (Dadina et al. 2005; Cappi et al. 2009; Tombesi et al. 2010). We searched, in fact, for such features in all 10 observations obtained after the *XMM-Newton* campaign, by including narrow absorption lines in the model between 4-10 keV. We found only a marginal ($\Delta\chi^2 \sim 6$) detection of two absorption features at 9 keV and 10.2 keV (rest-frame energies) during observation 4. Even if consistent with being produced by Fe XXVI Kα and Kβ at v$\sim$0.3c, and similar to earlier results (Cappi et al. 2009), the level of (highly) ionised absorption during the *XMM-Newton* campaign is found to be significantly reduced compared with most previous *XMM-Newton* observations. We obtained upper limits (at 90 % confidence) on the equivalent width of narrow (σ fixed to 100 eV) Gaussian absorption lines with typical values between -5 and -30 eV, between 7.5 and 9.0 keV, depending on the energy and observation considered. This is typically lower than values (between -20 and -30 eV) found in the lines detected in earlier observations (Cappi et al. 2009, Tombesi et al. 2010) excluding that such UFOs were present during the 2009 campaign.

5.1. Collisionally ionised plasma

We attempt to interpret the highly ionised emission lines via a self-consistent physical model. First we applied the collisionally ionised model CIE[3] in spex (Kaastra et al. 1996). In this fit we considered the 3.5–10 keV band for the continuum. We used Gaussian components for the Fe Kα line profile and Fe Kβ, constraining the flux of the latter to be 0.155-0.16 times the Fe Kα one (Palmeri et al. 2003). This was done in order

---

[3] http://www.sron.nl/files/HEA/SPEX/manuals/manual.pdf

to mitigate the degeneracy induced by the partial blend with the Fe XXVI Ly α line. The best fit points to a high-temperature gas (kT= 8.5±1.5 keV). At this temperature, the predicted line fluxes are $\sim 5 \times 10^{-6}$ ph cm^{-2} s^{-1} and $\sim 3 \times 10^{-6}$ ph cm^{-2} s^{-1} for the Fe XXV triplet and the Fe XXVI Ly α, respectively. These values are consistent with those measured empirically using Gaussian lines (i.e. Table 2). In theory these lines may be produced by hot, line emitting, gas in the form of a starburst driven wind. Mrk 509 has a total luminosity L$_{2-10\,\mathrm{keV}} = 1.3 \times 10^{44}$ erg s^{-1} in the 2-10 keV band. Assuming an Fe abundance of 0.4 Solar (as observed in starburst galaxies, Cappi et al. 1999) the best fit thermal starburst model requires a luminosity L$_{2-10\,\mathrm{keV}} = 3.3 \times 10^{42}$ erg s^{-1} to reproduce the Fe XXV and Fe XXVI line emission (reducing to L$_{2-10\,\mathrm{keV}} = 1.6 \times 10^{42}$ erg s^{-1} for Solar iron abundance). Using the correlation between L$_{2-10\,\mathrm{keV}}$ and the far infrared luminosity (L$_{\mathrm{FIR}}$), valid in star forming galaxies (Ranalli et al. 2003), we estimate a corresponding L$_{\mathrm{FIR}} > 10^{46}$ erg s^{-1} and a star formation rate higher than 400 M$_\odot$ yr^{-1}, which is several times larger than the actual total IR luminosity of Mrk 509, L$_{\mathrm{IR}} \sim 2 \times 10^{11}$ L$_\odot \sim 8 \times 10^{44}$ erg s^{-1} (Rieke et al. 1978), thus we disfavour this interpretation.

5.2. Photo-ionised plasma

Alternatively, the highly ionised lines may be produced by a photoionised plasma. To test this we used a grid of parameters created using Cloudy (Ferland et al. 1998) where the column density logN_{H} of the gas ranged between $21.7 - 24.5$ cm^{-2} and the ionisation parameter log(ξ) ranged between $3.4 - 7$. The grid has been calculated using a covering factor of one. Since the intrinsic line luminosity scales linearly with the covering factor, we used the ratio between the model and the data of the Fe XXVI line as a reference for the covering factor. In Mrk 509, only Fe XXVI and Fe XXV have significant detection, while for other narrow lines from highly ionised ions (e.g. O VIII at 18.97 Å and Ne X at 12.13 Å) we have obtained upper limits from the RGS spectrum. These limits are useful in constraining the model (i.e. Costantini et al. 2010). In Fig. 7 we compare the line luminosities observed with those computed for a range of models which can fit the data. In order to reproduce the luminosity of the highly ionised iron ions, the gas should have log(ξ)= $4 - 5.1$ and $N_{\mathrm{H}} = 23.4 - 24.2$. The covering factor is $C_V = 0.3 - 0.5$. As we do not see any associated absorption, the gas must be out of the line of sight. Such lines might possibly originate in e.g. the narrow line region or the highly ionised skin of the torus (Bianchi et al. 2005; Bianchi & Matt 2002).

5.3. Ionised reflection from inner disc

As shown in §3, the ionised emission can be fitted equally well with an ionised relativistic emission line. A comparably good fit is also obtained with a broad Gaussian Fe XXV profile in addition to the double Fe Kα +β lines. We fix the energy of the broad Fe XXV line to E= 6.7 keV. The line is significantly broadened $\sigma = 0.23$ keV and moderately intense (EW= 15 eV). Although this broadening is not as extreme as to exclude a simple Compton broadening on the ionised surface of the accretion disc, we decided, as an alternative to the Gaussian line, to fit the ionised emission with a relativistic disc line profile. An acceptable fit is obtained also in this case ($\chi^2 = 1204.7$ for 1192 dof). Assuming a standard disc emissivity index, inclination and outer disc radius of $\beta = -3$, $\alpha = 30°$ and $r_{\mathrm{out}} = 200$ r$_g$, the best fit disc inner
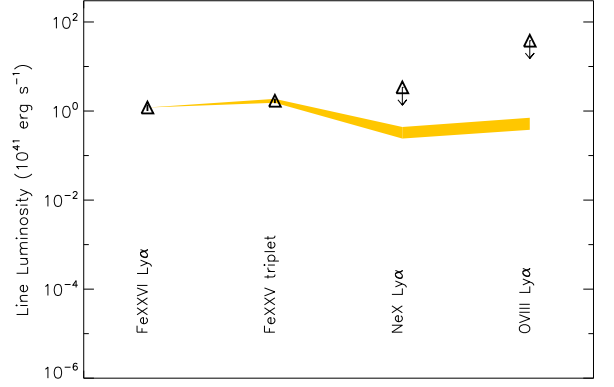

Fig. 7. Photoionization modeling for the highly ionized iron ions Fe XXVI and Fe XXV. Triangles: data. Light shaded line: range of models viable to fit the data.

radius is $r_{\mathrm{in}} = 27$ r$_g$, consistent with a value as small as $r_{\mathrm{in}} = 7$ r$_g$ and the disc-line equivalent width is, EW = 20^{+6}_{-8} eV.

It is difficult to estimate the line EW expected from an ionised inner annulus of the disc. In fact the Fe XXV and Fe XXVI line EW strongly depend on the poorly constrained disc ionisation parameter (Garcia et al. 2011) and on the disc annulus covering angle. However for reasonable values of these parameters (annulus covering angle $\sim 20 - 40$ % of the sky and log(ξ)$\sim 2.8 - 3.5$ erg cm^{-2} s^{-1}, which corresponds to the peak of Fe XXV and Fe XXVI emission) the line EW is expected to be between 5-50 eV. These results suggest that the inner part of the accretion disc might be highly ionised, thus explaining the lack of detection of relativistic Fe Kα line, combined with the high source efficiency (which suggests a thin standard accretion disc extending all the way down to the last stable orbit).

6. Discussion and Conclusions

We investigated the spectral variability of the Fe K band in the nearby, bright Seyfert 1 galaxy Mrk 509, using the 10 observations of the 2009 *XMM-Newton* monitoring campaign as well as all the previous *XMM-Newton* observations, totalling an exposure of more than 900 ks in about 10 years, resulting in one of the best quality Fe K spectra ever taken of a Seyfert 1 galaxy. This allows us, for the first time, to perform reverberation mapping of the resolved Fe Kα line.

Figure 8 summarise in a sketch a possible scenario for the production of the Fe K emission in Mrk 509. The width of the narrow core of the Fe Kα line suggests an origin from distant material, possibly the inner wall of the molecular torus located at 0.2-few pc. The correlated variations (on a few days time-scales) between the 3-10 keV continuum and the intensity of the resolved component of the Fe Kα suggest an origin between several tens and few thousands of r$_g$ from the BH. The resolved Fe Kα emission can be produced in the disc, but we favour an origin at the base of a stratified broad line region. We note that none of the X-ray or UV absorption components with measured location is co-spatial with the resolved Fe Kα emitting region. Moreover, the properties of the X-ray and UV absorbers appear to differ from the ones required to produce the resolved Fe Kα line, suggesting that this emitting material is outside the line of sight,
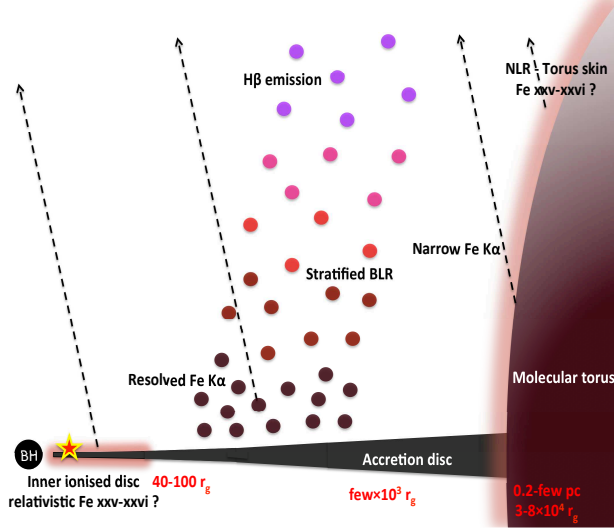
Fig. 8. Sketch of a possible locations for the different regions producing Fe K emission (diagram not to scale). The star represents the primary X-ray source, located close to the BH.

possibly in the form of an equatorial disc flattened wind such as observed in stellar mass black holes in the soft state (Ponti et. al. 2012) and neutron stars (Diaz-Trigo et al. 2006). The ionised Fe K emission might be produced either by photo-ionisation from distant material, such as the narrow line region and/or the ionised skin of the torus, or in the ionised inner accretion disc.

The results of this study show that:

– The *XMM-Newton* spectrum of Mrk 509 shows an evident Fe Kα line with total EW= 58 ± 4 eV. Fitted with a single Gaussian line the width is $\sigma = 0.092 \pm 0.012$ keV. The line intensity increases with the 3-10 keV flux, but not as strongly as expected in a constant EW scenario, suggesting the presence of a constant and a variable Fe Kα line component.

– The *Chandra* HETG spectrum has enough energy resolution to resolve the narrow component of the Fe Kα line ($\sigma = 0.027^{+0.018}_{-0.010}$ keV; line intensity $(1.5 \pm 0.2) \times 10^{-5}$ ph cm^{-2} s^{-1}). The width of the narrow component of the line suggests an origin at around 0.2-0.5 pc (~ 30000 r_g) from the BH. This value is of the same order of magnitude as the molecular sublimation radius, suggesting that the narrow component of the Fe Kα line might be produced as reflection from the inner walls of the molecular torus. If so, because of light travelling effects, the intensity of this component has to be constant on years time-scales. We assume the presence of a constant narrow Fe Kα line (as observed by *Chandra* HETG) and add a second, resolved (now observed to be broader $\sigma = 0.22 \pm 0.04$ keV), Fe Kα component with EW= 42^{+9}_{-4} eV. There is excess emission at 7.06 keV, consistent with being produced (at least in part) by the associated Fe Kβ emission.

– For the first time reverberation mapping of the resolved component of the Fe Kα line on timescales of several days-years was successfully performed. The intensity of the resolved Fe Kα component shows a significant ($\sim 4\sigma$) 1-to-1 correlation with the 3-10 keV flux variability, however the EW stays constant during the 9 years *XMM-Newton* observed the source. The robustness of this result is confirmed by the re-

sults of the rms spectra which, in a model independent way, show an excess of variability at E= 6.45 ± 0.08 keV. This excess of variability is consistent with being the resolved component of the Fe Kα line ($\sigma \lesssim 0.2$ keV) varying in such a way as to keep a constant EW= 71 ± 36 eV. No measurable lag of the reflected component is observed.

– The width of the resolved component of the Fe Kα line suggests an origin between 300 and 1000 r_g from the BH. This location is consistent with the observed Fe Kα variability on days to a week timescale and the lack of measurable lag. The lack of a relativistic red wing of the Fe Kα line suggests an inner radius for the line production larger than several tens of r_g (~ 40 r_g).

– The EW= 42^{+9}_{-4} eV of the resolved Fe Kα line suggests a larger covering factor of the primary X-ray sources (assumed to have altitudes of few r_g above the BH) compared to the one expected from a flat disc annulus, indicating a possible azimuthal distribution above the disc of the reflecting material. A possibility is that the material producing the resolved Fe Kα emission might be in the form of clouds, perhaps associated to the inner BLR (see Costantini et al. 2012). This geometry is further reinforced by the consistency between the Fe Kα line width ($\sigma = 0.22$ keV) and those from the broadest components of the UV broad emission lines (Kriss et al. 2011). We also observe that the location of the reverberating Fe Kα emission does not correspond to that of any X-ray or UV absorption components (Detmers et al. 2011; Kaastra et al. 2012; Kriss et al. 2011; 2012; Ebrero et al. 2011).

– Significant, but weak (15-20 eV) ionised Fe K emission is observed. The ionised emission can be fit equally well with two narrow emission lines (from both Fe XXV and Fe XXVI), possibly from a photo-ionised or collisionally ionised gas, or by a single broad relativistic emission line (either Fe XXV or Fe XXVI). We note that the source high Eddington ratio suggests the presence of a standard thin α-disc down to a few r_g from the BH. However, the neutral Fe Kα line has no redshifted wing with no neutral emission closer than ~ 40 r_g from the BH. This suggests that the surface of the inner accretion disc in Mrk 509 might be highly ionised. For these reasons, although the two interpretations for the origin of the ionised Fe K emission are equivalent on a statistical ground, we slightly prefer the latter interpretation on physical grounds. The picture of an higher ionised disc in the inner few tens of r_g from the BH and less ionised outside is in line with the presence of a compact hard X-ray corona, providing there a high flux of hard X-ray photons, and a soft more extended one, as proposed by Petrucci et al. (2012).

– A highly ionised, medium outflow velocity ($v \sim 0.048 \pm 0.013$ c) Fe K absorption component detected in previous observations (EW= $-13^{+5.9}_{-2.9}$ eV at ~ 4 σ significance) appears much weaker (EW= $-3.2^{+2.6}_{-2.8}$ eV, ~ 4 times weaker), if not absent, during the 2009 campaign.

– Previous *XMM-Newton* observations showed evidence for highly ionised high outflow velocity ($v \sim 0.05 - 0.2$ c) absorbers based on a total exposure of ~ 300 ks. We find no convincing ($> 3\sigma$) evidence for these features during the 2009 *XMM-Newton* long (600 ks) monitoring campaign.

Acknowledgments

References

Arav, N., Gabel, J. R., Korista, K. T., et al. 2007, ApJ, 658, 829
Avni, Y. 1976, ApJ, 210, 642
Barvainis, R. 1987, ApJ, 320, 537
Basko, M. M. 1978, ApJ, 223, 268
Begelman, M. C., & McKee, C. F. 1983, ApJ, 271, 89
Begelman, M. C., & McKee, C. F. 1983, ApJ, 271, 89
Bentz, M. C., Peterson, B. M., Pogge, R. W., & Vestergaard, M. 2009, ApJ, 694, L166
Bianchi, S., & Matt, G. 2002, A&A, 387, 76
Bianchi, S., Matt, G., Nicastro, F., Porquet, D., & Dubau, J. 2005, MNRAS, 357, 599
Bianchi, S., Guainazzi, M., Matt, G., & Fonseca Bonilla, N. 2007, A&A, 467, L19
Bianchi, S., Guainazzi, M., Matt, G., Fonseca Bonilla, N., & Ponti, G. 2009, A&A, 495, 421
Bianchi, S., Bonilla, N. F., Guainazzi, M., Matt, G., & Ponti, G. 2009, A&A, 501, 915
Blandford, R. D., & McKee, C. F. 1982, ApJ, 255, 419
Cappi, M., Tombesi, F., Bianchi, S., et al. 2009, A&A, 504, 401
Canizares, C. R., Davis, J. E., Dewey, D., et al. 2005, PASP, 117, 1144
Cerruti, M., Ponti, G., Boisson, C., et al. 2011, A&A, 535, A113
Clavel, J., Reichert, G. A., Alloin, D., et al. 1991, ApJ, 366, 64
Costantini, E., Kaastra, J. S., Korista, K., et al. 2010, A&A, 512, A25
Crenshaw, D. M., Kraemer, S. B., & George, I. M. 2003, ARA&A, 41, 117
Dadina, M., Cappi, M., Malaguti, G., Ponti, G., & de Rosa, A. 2005, A&A, 442, 461
de La Calle Pérez, I., Longinotti, A. L., Guainazzi, M., et al. 2010, A&A, 524, A50
de Marco, B., Iwasawa, K., Cappi, M., et al. 2009, A&A, 507, 159
de Marco, B., Ponti, G., Uttley, P., et al. 2011, MNRAS, 417, L98
De Marco, B., Ponti, G., Cappi, M., et al. 2011, arXiv:1201.0196
Detmers, R. G., Kaastra, J. S., Steenbrugge, K. C., et al. 2011, A&A, 534, A38 (paper III)
Díaz Trigo, M., Parmar, A. N., Boirin, L., Méndez, M., & Kaastra, J. S. 2006, A&A, 445, 179
Dovčiak, M., Bianchi, S., Guainazzi, M., Karas, V., & Matt, G. 2004, MNRAS, 350, 745
Ebrero, J., Kriss, G. A., Kaastra, J. S., et al. 2011, A&A, 534, A40 (paper V)
Emmanoulopoulos, D., McHardy, I. M., & Papadakis, I. E. 2011, MNRAS, 416, L94
Fabian, A. C., Iwasawa, K., Reynolds, C. S., & Young, A. J. 2000, PASP, 112, 1145
Fabian, A. C., Zoghbi, A., Ross, R. R., et al. 2009, Nature, 459, 540
Ferland, G. J., Korista, K. T., Verner, D. A., et al. 1998, PASP, 110, 761
Fruscione, A., McDowell, J. C., Allen, G. E., et al. 2006, Proc. SPIE, 6270,
Fukazawa, Y., Hiragi, K., Mizuno, M., et al. 2011, ApJ, 727, 19
García, J., Kallman, T. R., & Mushotzky, R. F. 2011, ApJ, 731, 131

Garmire, G. P., Bautz, M. W., Ford, P. G., Nousek, J. A., & Ricker, G. R., Jr. 2003, Proc. SPIE, 4851, 28
Huchra, J., Latham, D. W., da Costa, L. N., Pellegrini, P. S., & Willmer, C. N. A. 1993, AJ, 105, 1637
Iwasawa, K., Miniutti, G., & Fabian, A. C. 2004, MNRAS, 355, 1073
Kaastra, J. S., & Mewe, R. 1993, A&AS, 97, 443
Kaastra, J. S., Mewe, R., & Nieuwenhuijzen, H. 1996, UV and X-ray Spectroscopy of Astrophysical and Laboratory Plasmas, 411
Kaastra, J. S., Mewe, R., Liedahl, D. A., Komossa, S., & Brinkman, A. C. 2000, A&A, 354, L83
Kaastra, J. S., Petrucci, P.-O., Cappi, M., et al. 2011, A&A, 534, A36 (paper I)
Kaastra, J. S., Detmers, R. G., Mehdipour, M., et al. 2012, A&A, 539, A117 (paper VIII)
Kaspi, S., Smith, P. S., Netzer, H., et al. 2000, ApJ, 533, 631
King, A. L., Miller, J. M., & Raymond, J. 2012, ApJ, 746, 2
Kriss, G. A., Arav, N., Kaastra, J. S., et al. 2011, A&A, 534, A41 (paper VI)
Kriss, G. A., Arav, N., Kaastra, J. S., et al. 2012, arXiv:1201.1024
Krolik, J. H., & Kriss, G. A. 1995, ApJ, 447, 512
Krolik, J. H., & Kriss, G. A. 2001, ApJ, 561, 684
Landt, H., Elvis, M., Ward, M. J., et al. 2011, MNRAS, 414, 218
Laor, A. 1991, ApJ, 376, 90
Liu, Y., Elvis, M., McHardy, I. M., et al. 2010, ApJ, 710, 1228
Markowitz, A., Edelson, R., Vaughan, S., et al. 2003, ApJ, 593, 96
Malizia, A., Bassani, L., Zhang, S. N., et al. 1999, ApJ, 519, 637
Matt, G., Perola, G. C., & Piro, L. 1991, A&A, 247, 25
Matt, G., Fabian, A. C., & Reynolds, C. S. 1997, MNRAS, 289, 175
Matt, G., Brandt, W. N., & Fabian, A. C. 1996, MNRAS, 280, 823
McHardy, I. M., Koerding, E., Knigge, C., Uttley, P., & Fender, R. P. 2006, Nature, 444, 730
Mehdipour, M., Branduardi-Raymont, G., Kaastra, J. S., et al. 2011, A&A, 534, A39 (paper IV)
Miller, J. M., Raymond, J., Fabian, A., et al. 2006, Nature, 441, 953
Miller, L., Turner, T. J., Reeves, J. N., & Braito, V. 2010, MNRAS, 408, 1928
Molendi, S., Bianchi, S., & Matt, G. 2003, MNRAS, 343, L1
Murphy, E. M., Lockman, F. J., Laor, A., & Elvis, M. 1996, ApJS, 105, 369
Nandra, K., O'Neill, P. M., George, I. M., & Reeves, J. N. 2007, MNRAS, 382, 194
Nandra, K., George, I. M., Mushotzky, R. F., Turner, T. J., & Yaqoob, T. 1997, ApJ, 477, 602
Noda, H., Makishima, K., Yamada, S., et al. 2011, PASJ, 63, 925
Palmeri, P., Mendoza, C., Kallman, T. R., Bautista, M. A., & Meléndez, M. 2003, A&A, 410, 359
Palmeri, P., Mendoza, C., Kallman, T. R., & Bautista, M. A. 2003, A&A, 403, 1175
Page, M. J., Davis, S. W., & Salvi, N. J. 2003, MNRAS, 343, 1241
Peterson, B. M. 1993, PASP, 105, 247
Peterson, B. M., Ferrarese, L., Gilbert, K. M., et al. 2004, ApJ, 613, 682
Petrucci, P. O., Ponti, G., Matt, G., et al. 2007, A&A, 470, 889
Piconcelli, E., Jimenez-Bailón, E., Guainazzi, M., et al. 2005, A&A, 432, 15
Ponti, G., Cappi, M., Dadina, M., & Malaguti, G. 2004, A&A, 417, 451
Ponti, G., Miniutti, G., Cappi, M., et al. 2006, MNRAS, 368, 903
Ponti, G., Cappi, M., Vignali, C., et al. 2009, MNRAS, 394, 1487
Ponti, G., Gallo, L. C., Fabian, A. C., et al. 2010, MNRAS, 406, 2591
Ponti, G., Fender, R. P., Begelman, M. C., et al. 2012, MNRAS, L417
Ponti, G., Papadakis, I., Bianchi, S., et al. 2011, arXiv:1112.2744
Pounds, K., Reeves, J., O'Brien, P., et al. 2001, ApJ, 559, 181
Ranalli, P., Comastri, A., & Setti, G. 2003, A&A, 399, 39
Revnivtsev, M., Sazonov, S., Jahoda, K., & Gilfanov, M. 2004, A&A, 418, 927
Reynolds, C. S., Young, A. J., Begelman, M. C., & Fabian, A. C. 1999, ApJ, 514, 164
Reynolds, C. S., & Nowak, M. A. 2003, Phys. Rep., 377, 389
Rieke, G. H. 1978, ApJ, 226, 550
Sazonov, S., Revnivtsev, M., Krivonos, R., Churazov, E., & Sunyaev, R. 2007, A&A, 462, 57
Shakura, N. I., & Sunyaev, R. A. 1973, A&A, 24, 337
Steenbrugge, K. C., Kaastra, J. S., Detmers, R. G., et al. 2011, A&A, 534, A42 (paper V)
Tanaka, Y., Nandra, K., Fabian, A. C., et al. 1995, Nature, 375, 659
Tombesi, F., de Marco, B., Iwasawa, K., et al. 2007, A&A, 467, 1057
Tombesi, F., Cappi, M., Reeves, J. N., et al. 2010, A&A, 521, A57
Turner, T. J., Miller, L., George, I. M., & Reeves, J. N. 2006, A&A, 445, 59
Turner, T. J., Miller, L., Kraemer, S. B., & Reeves, J. N. 2011, ApJ, 733, 48
Vaughan, S., & Uttley, P. 2008, MNRAS, 390, 421
Yaqoob, T., & Padmanabhan, U. 2004, ApJ, 604, 63
Yaqoob, T., Reeves, J. N., Markowitz, A., Serlemitsos, P. J., & Padmanabhan, U. 2005, ApJ, 627, 156
Wilkins, D. R., & Fabian, A. C. 2011, MNRAS, 414, 1269
Woo, J.-H., & Urry, C. M. 2002, ApJ, 579, 530

Zoghbi, A., Fabian, A. C., Uttley, P., et al. 2010, MNRAS, 401, 2419

Zoghbi, A., & Fabian, A. C. 2011, MNRAS, 418, 2642

Zoghbi, A., Fabian, A. C., Reynolds, C. S., & Cackett, E. M. 2011, arXiv:1112.1717

2009 campaign - summed spectrum - 1 component of the Fe Kα line

		Fe Kα				Fe Kβ	Fe XXV		Fe XXVI		
Model	Γ	$E_{FeK\alpha}$ (keV)	$\sigma_{FeK\alpha}$ (keV)	$N_{FeK\alpha}$† (ph cm^{-2} s^{-1})	$EW_{FeK\alpha}$ (eV)	$EW_{FeK\beta}$ (eV)	$N_{Fe\ xxv}$† (ph cm^{-2} s^{-1})	$EW_{Fe\ xxv}$ (eV)	$N_{Fe\ xxvi}$† (ph cm^{-2} s^{-1})	$EW_{Fe\ xxvi}$ (eV)	χ^2/d.o.f.
(1)	1.66 ± 0.01	6.43 ± 0.01	0.14 ± 0.02	3.8 ± 0.3	70 ± 5						1311.7/1194
(2)	1.66 ± 0.01	6.43 ± 0.01	0.14 ± 0.02	3.8 ± 0.3	70 ± 5	$20 \pm 3\diamond$					1244.8/1193
(3)	1.66 ± 0.01	6.415 ± 0.012	0.092 ± 0.012	$3.2^{+0.3}_{-0.2}$	$58.3^{+5.0}_{-2.9}$	$10.4\ddagger$	$0.54^{+0.14}_{-0.18}$	9.8	$0.29^{+0.11}_{-0.13}$	6	1219.8/1192

		Fe Kα				Fe Kβ	Diskline				
	Γ	$E_{FeK\alpha}$	$\sigma_{FeK\alpha}$	$N_{FeK\alpha}$†	$EW_{FeK\alpha}$	$EW_{FeK\beta}$	incl. (deg.)	emissiv.	$N_{diskline}$† (ph cm^{-2} s^{-1})	$EW_{diskline}$ (eV)	χ^2/d.o.f.
(4)	1.67 ± 0.01	6.415 ± 0.011	0.084 ± 0.015	2.7 ± 0.2	50.0 ± 3.8	$8.2\ddagger$	33^{+4}_{-7}	$-2.2^{+0.5}_{-0.3}$	1.7 ± 0.5	36 ± 10	1216.0/1191
(5)	1.67 ± 0.01	6.425 ± 0.011	0.094 ± 0.018	2.9 ± 0.3	$53.8^{+6.2}_{-4.7}$	$8.6\ddagger$	18^{+4}_{-8}	-2.8 ± 0.3	$1.8^{+0.1}_{-0.5}$	40^{+22}_{-11}	1219.4/1191

Table 1. Best fit results of the summed EPIC-pn spectrum of the 10 *XMM-Newton* observations performed during the 2009 campaign. $\diamond$: assuming $\sigma_{Fe\ K\beta} = \sigma_{Fe\ K\alpha}$; $\ddagger$: assuming $\sigma_{Fe\ K\beta} = \sigma_{Fe\ K\alpha}$ and $N_{Fe\ K\beta} = 0.15 \times N_{Fe\ K\alpha}$; †: in units of 10^{-5} ph cm^{-2} s^{-1}.

- Model (1) *Single FeKα*: Power law + Gaus$_{FeK\alpha}$
- Model (2) *Single FeKα + β*: Power law + Gaus$_{FeK\alpha}$ + Gaus$_{FeK\beta}$
- Model (3) *Photo-ionised gas + Single FeKα + β*: Power law + Gaus$_{FeK\alpha}$ + Gaus$_{FeK\beta}$ + Gaus$_{FeXXV}$ + Gaus$_{FeXXVI}$
- Model (4) *Broad line$_{FeXXV}$ + Single FeKα + β*: Power law + Gaus$_{FeK\alpha}$ + Gaus$_{FeK\beta}$ + Diskline$_{FeXXV}$
- Model (5) *Broad line$_{FeXXVI}$ + Single FeKα + β*: Power law + Gaus$_{FeK\alpha}$ + Gaus$_{FeK\beta}$ + Diskline$_{FeXXVI}$

2009 campaign - summed spectrum - 2 components of the Fe Kα line

		Narrow Fe Kα			Resolved Fe Kα			Fe XXV		Fe XXVI		Absorption line		
Model	Γ	$E_{FeK\alpha}$ (keV)	$N_{FeK\alpha N}$† (phcm^{-2} s^{-1})	$EW_{FeK\alpha N}$ (eV)	$\sigma_{FeK\alpha R}$ (keV)	$N_{FeK\alpha R}$† (ph cm^{-2} s^{-1})	$EW_{FeK\alpha R}$ (eV)	$N_{Fe\,xxv}$† (ph cm^{-2} s^{-1})	$EW_{Fe\,xxv}$ (eV)	$N_{Fe\,xxvi}$† (ph cm^{-2} s^{-1})	$EW_{Fe\,xxvi}$ (eV)	E_{abs}	N_{abs}† (ph cm^{-2} s^{-1} : eV)	χ^2/d.o.f.
(6)	1.67 ± 0.01	6.420 ± 0.010	1.5†	27†	0.22 ± 0.04	$2.33^{+0.38}_{-0.27}$	42^{+9}_{-4}	0.21 ± 0.15	3.9 ± 2.7	0.20 ± 0.13	4.2 ± 2.6	7.31 ± 0.1	$-0.15 \pm 0.12 : 3.4 \pm 2.7$	1197.9/1190

2000 - 2006 *XMM-Newton* observations - summed spectrum - 2 components of the Fe Kα line

		Narrow Fe Kα			Resolved Fe Kα			Fe XXV		Fe XXVI		Absorption line		
(6)	1.67 ± 0.01	6.427 ± 0.014	1.5†	33†	$0.21^{+0.12}_{-0.07}$	$1.50^{+0.60}_{-0.38}$	33^{+6}_{-7}	< 0.47	< 10.4	0.37 ± 0.18	9.5 ± 4.5	7.34 ± 0.05	$-3.6 \pm 0.2 : 10.1 \pm 3.8$	1212.3/1190

Table 2. †: in units of 10^{-5} ph cm^{-2} s^{-1}.

2009 campaign - summed spectrum - 2 components of the Fe Kα line

		Narrow Fe Kα			Resolved Fe Kα			Diskline			
Model	Γ	$E_{FeK\alpha}$ (keV)	$N_{FeK\alpha N}$† (ph cm^{-2} s^{-1})	$EW_{FeK\alpha N}$ (eV)	$\sigma_{FeK\alpha R}$ (keV)	$N_{FeK\alpha R}$† (ph cm^{-2} s^{-1})	$EW_{FeK\alpha R}$ (eV)	$\sigma_{ion.}$ (keV)	$N_{ion.}$ (ph cm^{-2} s^{-1})	$EW_{ion.}$ (eV)	χ^2/d.o.f.
(7)	1.67 ± 0.01	6.416 ± 0.011	1.5†	27†	$0.23^{+0.05}_{-0.04}$	$2.02^{0.54}_{-0.32}$	36^{+9}_{-6}	$0.23^{+0.1}_{-0.06}$	$0.79^{+0.66}_{-0.40}$	15^{+12}_{-8}	1203.5/1192
								r_{in} (r_g)	N_{disk} (ph cm^{-2} s^{-1})	$EW_{ion.}$ (eV)	χ^2/d.o.f.
(8)	1.67 ± 0.01	6.425 ± 0.013	1.5†	27†	$0.21^{+0.07}_{-0.03}$	$1.92^{+0.85}_{-0.27}$	34^{+15}_{-5}	27^{+41}_{-20}	$0.92^{+0.46}_{-0.36}$	20^{+6}_{-9}	1204.7/1192

Table 3. †: in units of 10^{-5} ph cm^{-2} s^{-1}.

– Model (6) *Photo-ionised gas + Double FeKα + Absorption line*: Power law + Gaus$_{FeK\alpha N}$ + Gaus$_{FeK\alpha R}$ + Gaus$_{FeK\beta N}$ + Gaus$_{FeK\beta R}$ + Gaus$_{FeXXV}$ + Gaus$_{FeXXVI}$ - AbsGaus

– Model (7) *Broad ionised Gaussian*$_{FeXXVI}$ + *Double FeKα*: Power law + Gaus$_{FeK\alpha N}$ + Gaus$_{FeK\alpha R}$ + Gaus$_{FeK\beta N}$ + Gaus$_{FeK\beta R}$ + Gaus$_{FeXXV}$ + Gaus$_{FeXXVI}$ - AbsGaus
– Model (8) *Ionised-disc-line*$_{FeXXVI}$ + *Double FeKα* : Power law + Gaus$_{FeK\alpha N}$ + Gaus$_{FeK\alpha R}$ + Gaus$_{FeK\beta N}$ + Gaus$_{FeK\beta R}$ + Gaus$_{FeXXV}$ + Gaus$_{FeXXVI}$ - AbsGaus